Available online at www.sciencedirect.com
SCIENCE DIRECT
Journal of Photochemistry and Photobiology A: Chemistry 178 (2006) 192–200
Journal of Photochemistry and Photobiology A:Chemistry
www.elsevier.com/locate/jphotochem

Femtosecond fluorescence spectroscopy and near-field spectroscopy of water-soluble tetra(4-sulfonatophenyl)porphyrin and its J-aggregate

Atsushi Miura [a,1], Yutaka Shibata [b,2], Haik Chosrowjan [b], Noboru Mataga [b], Naoto Tamai [a,*]

[a] *Department of Chemistry, School of Science and Technology, Kwansei Gakuin University, 2-1 Gakuen, Sanda 669-1337, Japan*
[b] *Institute for Laser Technology, 18-4 Utsubo-Hommachi, Nishi-ku, Osaka 550-0004, Japan*

Available online 27 December 2005

Abstract

Fluorescence dynamics of tetra(4-sulfonatophenyl)porphyrin (TPPS) in aqueous solution and mesoscopic structures of TPPS in thin films have been investigated by femtosecond fluorescence up-conversion spectroscopy and scanning probe microscopy (AFM/SNOM), respectively. We observed very short lifetime in *B*-state fluorescence of J-aggregate (140 ± 10 fs) which was shorter than that of monomer (200 ± 10 fs) and protonated monomer (530 ± 10 fs). In addition to the very short lifetime component in *B* state, we found very weak and short lifetime component in *Q* state of monomer TPPS. Fluorescence observed at the shorter wavelength edge of the monomer *Q* band has a comparable short lifetime of 240 ± 20 fs as well as *B*-state component which has been assigned to the fluorescence from $Q_y(0, 0)$ state. TPPS J-aggregate prepared by spin coating on the substrate shows quasi-2D nano-rod structures originated from the interaction between 1D J-aggregate. Large microcrystalline structures were observed in drop cast film. Near-field absorption and fluorescence images suggest the structural inhomogeneities of J-aggregate microcrystals.

Keywords: Tetra(4-sulfonatophenyl)porphyrin; J-aggragate; Fluorescence up-conversion spectroscopy; Scanning near-field optical microscopy

1. Introduction

Since the discovery of the J-aggregates by Scheibe [1] and Jelley [2], the optical properties of these molecular systems have attracted great interest. Cyanine dyes are typical compounds to form J-aggregates, and some porphyrin derivatives are also known to form J-aggregates [3–8]. The photophysical properties of porphyrin aggregates have been extensively investigated by various spectroscopic techniques because of the structural and spectral similarities between porphyrin and chlorophylls that play a vital role in nature such as photosynthetic systems [9,10]. Thus, the porphyrin J-aggregate is a useful model compound for studying the excited-state dynamics of the organisms. In several papers, one-dimensional (1D) Frenkel exciton structure, in which the transition dipole moment of porphyrins is aligned with "head-to-tail" orientation and strongly interacted each other, is proposed for the structural model of TPPS J-aggregate [3–7,11]. Because of the nature of dipole–dipole interaction between molecules, the characteristics of J-aggregates are strongly dependent on the ordering of molecular arrangements.

J-aggregates of the dye molecules have been drawing interests due to their peculiar photophysical properties for potential applications such as opto-electronic devices. For such kind of application of J-aggregate, 1D linear aggregates (or 1D Frenkel excitons) should be transferred on two-dimensional (2D) plane of solid substrate. Therefore, information on photophysical properties of dye aggregates in 2D plane is indispensable for various applications. One of the most fruitful optical spectroscopic techniques in small domains is scanning near-filed optical microscopy (SNOM), which provides a spatial resolution better than the diffraction limit ($\lambda/2$) for imaging and spectroscopy applications [12]. High spatial resolution of SNOM enables us to make the characterization of optical properties and mesoscopic structures of dye aggregates in small domains [13,14]. For example, J-aggregates of pseudoisocyanine (PIC) dyes have been investigated by Barbara and co-workers using fluorescence, time-resolved fluorescence, and polarization SNOM techniques [15,16]. They observed several different shapes of long and fibrous structures of PIC J-aggregate on solid substrate.

* Corresponding author. Tel.: +81 79 565 8357; fax: +81 79 565 8357.
E-mail address: tamai@ksc.kwansei.ac.jp (N. Tamai).
[1] Present address: Graduate School of Materials Science, Nara Institute of Science and Technology, 8916-5 Takayama, 630-0192 Ikoma, Japan.
[2] Present address: Graduate School of Science, Nagoya University, Furo-cho, Chikusa-ku, Nagoya 464-8602, Japan.

1010-6030/$ – see front matter © 2005 Elsevier B.V. All rights reserved.
doi:10.1016/j.jphotochem.2005.10.037

In addition, the extent of excitation migration along J-aggregate was estimated to be less than ∼50 nm from the analysis of photobleaching induced by the incident light from the SNOM tip.

Another aspect of interesting photophysical property of porphyrins is the violation of Kasha's rule: some porphyrins emit the fluorescence from both secondly and lowest excited singlet states [17]. The fluorescence from the organic dye molecules usually occurs from the lowest excited singlet state (*Q* state or S_1 state) independent of the level of the excited state. Some porphyrins are known to emit the fluorescence from the secondly excited state (*B* state or S_2 state). Recently, several reports have been published on the *B*-state fluorescence dynamics of porphyrin derivatives by means of femtosecond fluorescence up-conversion and other techniques [18–21], although the direct measurement of the dynamics of the *B* state is difficult due to very weak fluorescence intensity and short fluorescence lifetime.

In the present study, we have investigated the fluorescence dynamics of water-soluble porphyrin, 5,10,15,20-tetraphenyl-21H,23H-porphinetetrasulfonic acid (TPPS). TPPS is one of the porphyrin derivatives to form J-aggregate in aqueous media depending on experimental conditions such as pH, dye concentration, and/or ionic strength [3–8], and shows fluorescence from the secondary excited state (*B* state). We have conducted the time-resolved fluorescence measurements of *B* and *Q* states for all species of TPPS, monomer, protonated monomer and J-aggregate, to elucidate the fluorescence dynamics of the *B* state. In addition to the photophysical properties of 1D linear aggregate in aqueous solution, we have investigated the mesoscopic structures and spectroscopic characteristics of TPPS J-aggregates on a solid substrate by means of atomic force microscopy (AFM) and scanning near-field optical microspectroscopy. We have also demonstrated near-field absorption and fluorescence spectroscopy on single assembly of TPPS J-aggregate.

2. Experimental

2.1. Materials

TPPS was purchased from Tokyo Kasei Co. and used without further purification. The chemical structure of monomer and protonated monomer of TPPS are shown in Fig. 1. Water for sample preparation was purified by a water purification system (Yamato Co., Millipore WQ500) to the resistivity of ∼18 MΩ cm. The pH of a sample solution was adjusted by adding 2N NaOH solution or concentrated HCl (Wako Chemical Co., super special grade, 35%) in order to change the molecular species of TPPS in aqueous solution. The concentration change of the sample solution caused by the pH adjustment is negligibly small because of the volume change less than 2%. The concentration of the sample solution was varied from 1.0×10^{-6} to 1.0×10^{-4} M depending on the experiments.

2.2. Steady-state and time-resolved spectroscopy

Steady-state absorption and fluorescence spectra were recorded with U-3210 spectrometer (Hitachi) and FluoroMax-2 (Jobin-Yvon, SPEX) spectrofluorimeter, respectively. In the

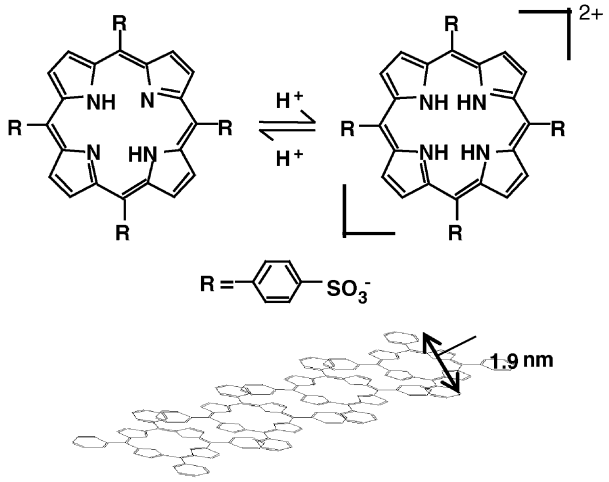

Fig. 1. Chemical structures of TPPS monomer (left) and TPPS protonated monomer (right). Proposed one-dimensional aggregate of TPPPS is depicted in lower panel.

fluorescence quantum yield measurements, rhodamine B was used as a standard sample [22]. Time-resolved fluorescence decay curves were measured by using a femtosecond fluorescence up-conversion apparatus. Detailed experimental set-up is described elsewhere [18]. Briefly, the sample was excited with the second harmonic of Ti:sapphire laser (Mira 900, Coherent, 810 nm, 76 MHz) pumped with a CW Ar-ion laser (Innova 310, Coherent). The sum-frequency signal of fluorescence and residual fundamental laser pulse of Ti:sapphire laser was detected with a photon-counting system (Hamamatsu, C5410). A cross-correlation signal between fundamental and its second harmonic pulses was used as an instrument response function (FWHM ≈ 200 fs). In the fluorescence up-conversion measurements, the sample solution was allowed to flow through a 2-mm flow cell using a magnetic gyre pump (Micropump, 040-332) to avoid any possibility of sample damage during the measurements. A non-linear least-squares iterative convolution method based on a Marquardt algorithm was used for the decay curve analysis [23].

2.3. Mesoscopic structure by scanning probe microscopy

Thin films of TPPS were prepared on a glass substrate by spin coating and drop casting of the sample solution. AFM measurements were performed with an Explorer AFM (Topometrix) operating in non-contact mode using silicon cantilever tips. The SNOM and near-field spectrum measurement was conducted by using the time-resolved fluorescence SNOM system based on Aurora (Topometrix). The details of the SNOM system is described elsewhere [13,14]. In brief, an Al-coated fiber tip with an aperture diameter of 50–100 nm was used. A SHG of Ti:sapphire laser and femtosecond white-light continuum generated by focusing an amplified Ti:sapphire laser into a water cell were used for fluorescence imaging, near-field fluorescence spectrum, and near-field absorption spectrum detections. Each light source with a power less than 1 mW was coupled into the cleaved end of the fiber. A near-field absorption

spectrum was obtained by a combination of a polychromator (Chromex, ChromSpec 250i) and a liquid nitrogen cooled multichannel detector (Princeton Instruments, CCD-1100). All the measurements were done under ambient conditions at room temperature.

3. Results and discussion

3.1. Steady-state spectroscopy

Fig. 2 illustrates the steady-state absorption and fluorescence spectra of TPPS at various conditions. The conformation of TPPS in aqueous solution can be controlled by adjusting the pH value of the solution. At relatively high pH region, typically above pH 4.5 at 1×10^{-5} M concentration of solution, TPPS exists as a monomer. Two out of four pyrrole rings are protonated and the rests are unprotonated, resulting in the D_{2h} symmetry [17]. Fig. 2a depicts the absorption spectrum of TPPS monomer, which shows the *B*-state absorption at 410 nm and four *Q*-band peaks at 515, 551, 579, and 633 nm, which is typical for D_{2h} free-base porphyrins. With decreasing the pH value less than 4, the unprotonated pyrrole rings are protonated to form the protonated monomer of TPPS possessing D_{4h} symmetry (Fig. 1). The absorption spectrum of the protonated monomer shows *B*-state absorption peak at 434 nm and two *Q*-band peaks at 594 and 644 nm (Fig. 2b). Two-banded absorption of the *Q* band is characteristic for the D_{4h} symmetry porphyrins such as metalloporphyrins. Further decreasing of pH value (pH < 2.2) induces red-shifted absorption peaks at 490 and 706 nm with the diminishing the protonated monomer absorption (Fig. 2c). This very sharp and large red-shifted absorption are characteristic of the J-aggregate. The spectral width of J-aggregate at *B* band is twice narrower than that of protonated monomer: ~350 cm^{-1} FWHM for J-aggregate and ~880 cm^{-1} FWHM for protonated monomer, respectively.

The fluorescence spectra of respective forms are illustrated in Fig. 2 with dotted lines. The fluorescence spectrum of monomer exhibits two peaks at 644 and 703 nm corresponding to $Q_x(0, 0)$ and $Q_x(0, 1)$, respectively, while single peaked spectra are observed for protonated monomer (~670 nm) and for J-aggregate (~714 nm). In addition to the *Q*-state fluorescence, we have observed very weak and sharp fluorescence from the *B* state for all species. Monomer, protonated monomer, and J-aggregate have *B*-state fluorescence peaks at 421, 446, and 495 nm, respectively. The Stokes shift in *B* state is very small: 520, 620, and 206 cm^{-1}, for monomer, protonated monomer, and J-aggregate, respectively. It should be noted that the presented fluorescence spectrum of the J-aggregate in Fig. 2c was excited at 460 nm, however, we could obtain the identical spectral feature for both *B* and *Q* states of J-aggregate in case of 400 nm excitation which applied for fluorescence up-conversion measurement (spectrum is not shown). In addition to the successful *B*-state fluorescence observation for all species, we have observed the very weak shoulder at higher energy side (580–620 nm) of the *Q* band of monomer. This emission is hardly recognized in linear scale plot but can be recognized in the logarithmic scale plot as illustrated in Fig. 3a. This very weak fluorescence will be discussed later.

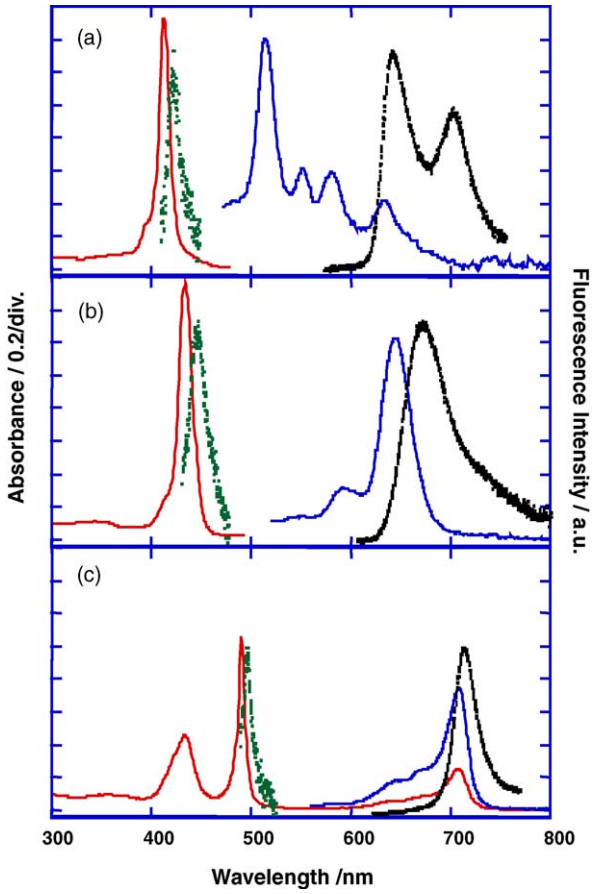

Fig. 2. Absorption (solid line, 1×10^{-5} M, optical path length; 3 mm) and fluorescence (dashed line, 5×10^{-6} M) spectra of TPPS in aqueous solution at various pH conditions: (a) pH 11.0, (b) pH 3.0, and (c) pH 1.0. Fluorescence spectra were measured with the excitation wavelength at (a) 400 nm, (b) 425 nm, and (c) 460 nm.

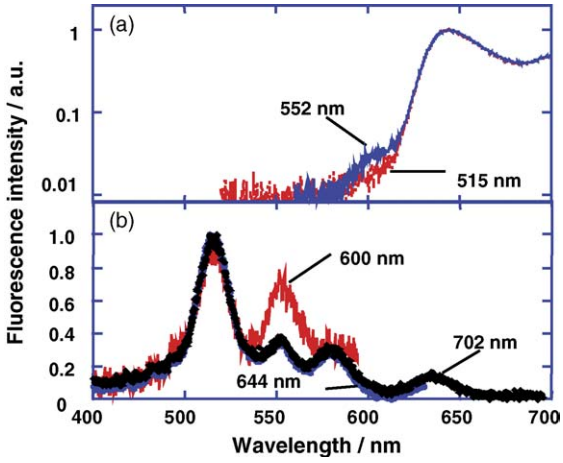

Fig. 3. (a) Fluorescence spectra of TPPS monomer excited at 515 and 552 nm in the *Q*-band region. Fluorescence intensity is normalized at the peak wavelength of 644 nm, and the vertical axis is shown in the logarithmic scale. (b) Fluorescence excitation spectra of TPPS monomer observed at 600, 644, and 702 nm. The spectra are normalized at the peak wavelength of 515 nm.

Table 1
Fluorescence quantum yields, lifetimes, and radiative rate constants of TPPS

Species	Quantum yield, Φ_f		Fluorescence lifetime, τ_f			Radiative rate constant, k_f[a]	
	B band (10^{-5})	*Q* band	*B* band	*Q* band		*B* band (s^{-1})	*Q* band (s^{-1})
			Decay (fs)	Rise (fs)	Decay (ns)		
Monomer	3.0	0.076	200 ± 10 (435 nm)	250 ± 40 (640 nm)	10.9 (645 nm), 210 ± 30 fs (600 nm)	1.5×10^8	7.0×10^6
Protonated monomer	11.0	0.083	530 ± 10 (470 nm)	680 ± 50 (660 nm)	3.9 (670 nm)	2.1×10^8	2.1×10^7
J-aggregate	9.1	0.001	140 ± 10 (500 nm)	210 ± 20 (730 nm)	0.055 (75%), 0.36 (15%) (720 nm)	6.5×10^8	1.8×10^7[b] (9.5×10^6)[c]

[a] $k_f = \Phi_f/\tau$.
[b] This value was calculated with 55 ps, main component of J-aggregate.
[c] This value was calculated with 106 ps which is an averaged lifetime of 55 and 360 ps decay components of J-aggregate.

The intensity of the *B*-state fluorescence is three orders of magnitude smaller than that of the *Q*-state fluorescence. The fluorescence quantum yields (Φ) of the respective species were estimated by using the following equation:

$$\Phi_i = \Phi_s \frac{F_i}{F_s} \frac{1 - 10^{-A_s}}{1 - 10^{-A_i}} \frac{n_i^2}{n_s^2} \quad (1)$$

where F is the integrated fluorescence intensity, A the optical density, n the refractive index of the solvent, and subscripts i and s are the sample and standard, respectively. The results of quantum yields (Φ_f) for both the *Q* and *B* states are summarized in Table 1. The examined $\Phi_f(Q)$ of the monomer (0.076) is in agreement with the reported value of 0.080 [24], which is comparable to protonated monomer ($\Phi_f(Q) \approx 0.083$) and much larger than that of the J-aggregate ($\Phi_f(Q) \sim 0.001$). In contrast to *Q*-state fluorescence, the fluorescence quantum yield of J-aggregate in *B* state ($\sim 9.1 \times 10^{-5}$) is larger than that of monomer ($\sim 3.0 \times 10^{-5}$) and comparable to that of protonated monomer ($\sim 1.1 \times 10^{-4}$).

3.2. Time-resolved fluorescence spectroscopy

The fluorescence lifetimes of respective species in the *Q* state were analyzed by picosecond single-photon timing ($\lambda_{ex} \approx 400$ nm) and the results are listed in Table 1. Obtained fluorescence lifetimes of monomer (10.9 ns) and protonated monomer (3.95 ns) are in good agreement with the reported values for monomer (9.26 ns, Maiti et al.; 9.5 ns, Akins et al.) and protonated monomer (3.87 ns, Maiti et al.; 3.9 ns, Akins et al.) [6,7]. The fluorescence decay of the J-aggregate could be fitted with a sum of three exponential decay function with lifetimes of 55 ps (75%), 360 ps (15%), and 3.4 ns (10%). The longest component is considered to be due to the overlap of the protonated monomer. Therefore, the short components of 55 and 360 ps are assigned to the decay components of J-aggregate.

Fluorescence dynamics of the *B* state was analyzed by the fluorescence up-conversion technique. Fig. 4 depicts the fluorescence decay curves of the *B* and *Q* states of monomer, protonated monomer, and J-aggregate. The decay curves of the *B*-state fluorescence for all species could be fitted with a single exponential

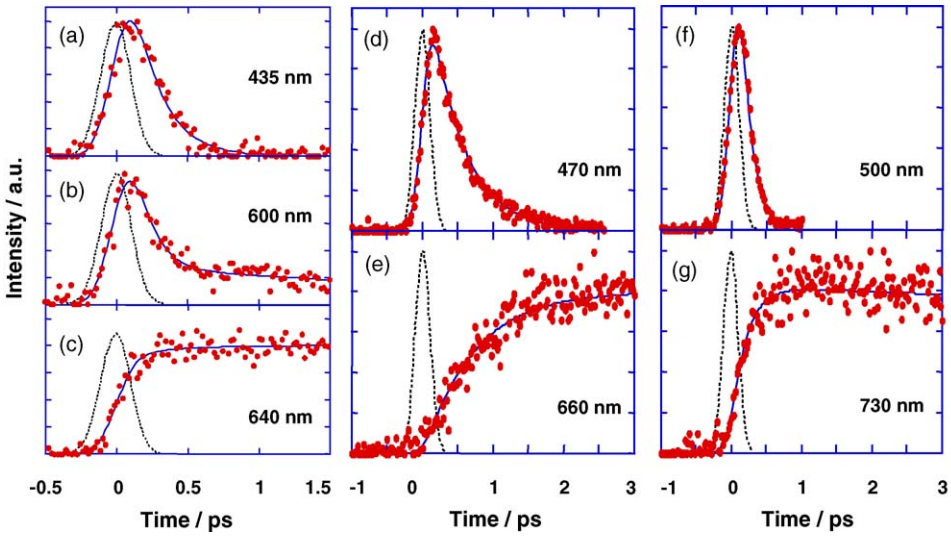

Fig. 4. Fluorescence rise and decay curves of TPPS monomer, protonated monomer, and J-aggregate. The sample is excited at 400 nm (SHG of Ti:sapphire laser). For monomer, the rise and decay profiles were observed at (a) 435 nm, (b) 600 nm, and (c) 640 nm. For protonated monomer, the rise and decay profiles were measured at (d) 470 nm and (e) 660 nm. For J-aggregate, the rise and decay curves were observed at (f) 500 nm and (g) 730 nm. The closed circles depict the experimentally observed fluorescence decay/rise profiles. The dashed and solid lines depict the system response function and convolution curves with a sum of exponential function, respectively.

decay function. No rise component was detected in our temporal resolution. Fig. 4a and c depicts the *B*-state fluorescence decay and *Q*-state rise/decay curves of the monomer. The lifetime of monomer in the *B* state was analyzed to be 200 ± 10 fs, which is in agreement with the rise component of the *Q*-state fluorescence (250 ± 40 fs) detected at 640 nm. The decay curves of the protonated monomer are depicted in Fig. 4d and e, in which the lifetime of the *B* state was estimated to be 530 ± 10 fs and the rise component of the *Q*-state fluorescence was 680 ± 50 fs. Fluorescence lifetime of the *B* state of J-aggregate was obtained as 140 ± 10 fs and the corresponding rise component of the *Q*-state fluorescence was 210 ± 20 fs (Fig. 4f and g). Fluorescence lifetime of J-aggregate is shortest in all species of TPPS. We found another very fast decay component in *Q* state of the monomer as shown in Fig. 4b. The fluorescence decay curve measured at 600 nm, which corresponds to very weak emitting component observed in fluorescence spectrum of the monomer at higher energy region (580–620 nm) of the *Q* state, showed two-exponential decay behavior with an ultrafast component of 210 ± 30 fs and a slow component of a few to tens of picoseconds without rise component.

We have calculated the radiative rate constants of all species by using respective fluorescence quantum yields and fluorescence lifetimes for both *B* and *Q* states. The results are summarized in Table 1. In the J-aggregate, the radiative rate constant of the *B* state, $k_f(B)$, is several times larger than that of the constituent, protonated monomer. In contrast to the *B* state, $k_f(Q)$ of the J-aggregate is comparable or smaller than that of the protonated monomer. The non-radiative rate constant of the *B* state of J-aggregate $k_n(B)$ is estimated to $\sim 7.1 \times 10^{12}\ s^{-1}$, which is several times larger than that of the protonated monomer ($\sim 1.9 \times 10^{12}\ s^{-1}$).

Discussion is now turned to the difference of observed *B*-state lifetime between monomer, protonated monomer and J-aggregate. Fluorescence from the higher excited *B* state of porphyrin is due to the competition with the internal conversion from *B* state to *Q* state. Several reasons considered here are the degeneration of excited electronic configuration and parallel energy surface configuration between *B* and *Q* states, the lack of allowed excited triplet states, and suppression of vibronic coupling between *B* and *Q* states because of relatively large energy gap. Observed *B*-state fluorescence lifetime of monomer (200 fs) is much shorter than that of protonated monomer (530 fs). The energy separation between *B* and *Q* states of monomer and protonated monomer is calculated to be $5.0 \times 10^3\ cm^{-1}$ for monomer and $7.5 \times 10^3\ cm^{-1}$ for protonated monomer. The wider energy separation in protonated monomer implies the lower density of vibronic states that contributes to the radiationless vibronic coupling between the *B* and *Q* states. Therefore, protonated monomer results in the longer fluorescence lifetime in *B* state than monomer.

B-state fluorescence lifetime of J-aggregate (140 fs) is shorter than that of protonated monomer. The lifetime of protonated monomer and J-aggregate should be similar because of the following reasons: (1) the difference of energy gap of *B* and *Q* states of J-aggregate ($6.3 \times 10^3\ cm^{-1}$) and protonated monomer is not so larger than that for monomer and protonated monomer and (2) J-aggregate is composed with the same constituent of protonated monomer. However, the fluorescence lifetime shows the obvious difference between two species even though these species have comparable fluorescence quantum yields, and the fluorescence lifetime of J-aggregate is much shorter than that of monomer. Faster internal conversion on J-aggregate may be explained by the larger radiative rate constant of J-aggregate. The enhancement of radiative rate in J-aggregate, which is due to the collective nature of the excited state of the aggregate, is well known as superradiance [25–29]. A typical example is the J-aggregate of pseudoisocyanine (PIC), in which the enhancement factor is about 100 at low temperature [30,31]. In the case of TPPS J-aggregate, the radiative rate constant of protonated monomer and J-aggregate in *Q* state is almost comparable, thus the enhancement in the *Q* state at room temperature is almost negligible. This is probably due to the weak transition dipole–transition dipole interaction in the *Q* state, which is completely different from the PIC J-aggregate. In contrast to the *Q* state, enhancement of the radiative rate constant of J-aggregate in the *B* state was observed because of the large transition dipole–transition dipole interaction, although the exciton scattering easily occurs at high temperatures and thus the enhancement factor is not large as that at low temperature. Thus, the internal conversion from the *B* state to the *Q* state is expected to be much faster in J-aggregate than in protonated monomer.

We should consider the origin of the very weak and ultrafast decay component at higher energy region (580–620 nm) in the *Q* band of the monomer (Fig. 3a). The fluorescence decay at 600 nm (Fig. 4c) has very fast component of 210 fs. As we described above, TPPS monomer has the D_{2h} symmetry and includes two electronic states in *Q* band, Q_x and Q_y states. Recently, Akimoto et al. have found similar ultrafast decay component at higher energy edge of the *Q* state of free-base porphyrin (H_2P) by fluorescence up-conversion technique [20]. This short lifetime component showed peaks at 560–600 nm which gave the mirror image relationship to the Q_y absorption. They proposed that the emission in this region is due to the fluorescence from the Q_y state and the internal conversion of $Q_y \rightarrow Q_x$ is probably the origin of the short lived component.

Fig. 3b depicts the steady-state excitation spectra of *Q* state observed at 600, 644, and 702 nm. The enhancement of the relative intensity of the $Q_y(0, 0)$ (peak at 552 nm) was observed with the detection at 600 nm. A similar phenomenon was observed in the fluorescence spectra (Fig. 3a). The $Q_y(0, 0)$ band excitation at 552 nm leads to slight enhancement of the fluorescence intensity around 600 nm as compared to the $Q_y(1, 0)$ excitation at 515 nm or the *B*-band excitation. There are two possible origins of this ultrafast decay component at 600 nm. One is originated from $Q_y(0, 0)$ state and the other is originated from a higher vibrational level of Q_x state. In the latter case, 600 nm fluorescence should be assigned to $Q_x(2, 0)$ or higher vibrational level. However, $Q_x(2, 0)$ or higher level absorption is weaker than $Q_y(0, 0)$ and $Q_y(1, 0)$ absorption, and the probability of $Q_x(2, 0)$ fluorescence should be weaker than $Q_y(1, 0)$ and $Q_y(0, 0)$ fluorescence. Furthermore, steady-state fluorescence spectrum measurements show wavelength dependence as described above. Therefore, it is more plausible that $Q_y(0, 0)$

state is the candidate of the origin of ultrafast decay component at 600 nm. The wavelength dependence may be explained by the competition between the transition from $Q_y(1, 0)$ to Q_x state and the relaxation from $Q_y(1, 0)$ to $Q_y(0, 0)$. After the B-state excitation, the internal conversion to higher vibrational levels of Q_y state takes place followed by the vibrational relaxation to $Q_y(1, 0)$ state, and then $Q_y(1, 0)$ to $Q_y(0, 0)$ relaxation leading to the fluorescence at 600 nm competes to $Q_y(1, 0)$ to Q_x transition. Thus, the excitation higher than $Q_y(1, 0)$ state shows rather weak fluorescence intensity at 600 nm than the direct excitation to $Q_y(0, 0)$ state. Moreover, the fluorescence band at 600 nm possess a mirror image relationship to $Q_y(0, 0)$ absorption spectrum. This weak fluorescence, therefore, assigned to the fluorescence from $Q_y(0, 0)$.

Fluorescence dynamics at 600 nm shows no rise component although the B state has very fast decay component of ∼210 fs. This can be simply explained by the consecutive reaction from B state to Q_y, and to Q_x state. The dynamics of B and Q_y states are given by the following equations:

$$B = B_0\, e^{-(k_1+k_B)t} \tag{2}$$

$$Q_y = \frac{k_1 B_0}{k_2 + k_{Q_y} - k_1 - k_B}\{e^{-(k_1+k_B)t} - e^{-(k_2+k_{Q_y})t}\} \tag{3}$$

where k_1 and k_2 are the rate constants from B to Q_y and Q_y to Q_x. k_B, k_{Q_y}, and k_{Q_x} are the rate constants from respective states to the ground state including the radiative rate constant. If $k_{Q_y} + k_2$, is larger than $k_B + k_1$, the dynamics of Q_y shows almost no rise component and the decay constant is comparable to that of the B state. The rise/decay behavior of each state is schematically summarized in Fig. 5a and b. This explains well

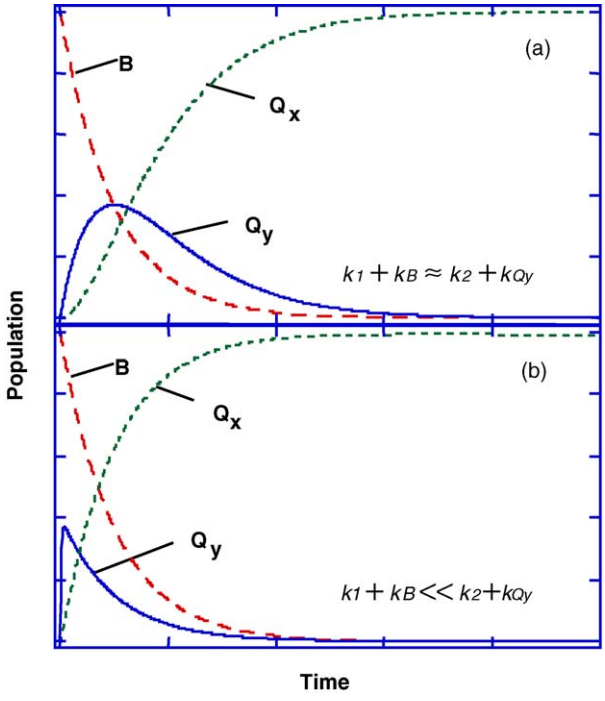

Fig. 5. Schematic drawing of the simulation results of consecutive reactions of three states (B, Q_x, and Q_y states). The population changes of each state were calculated with (a) $k_1 + k_B \approx k_2 + k_{Q_y}$ and (b) $k_1 + k_B \ll k_2 + k_{Q_y}$.

the observed fluorescence dynamics of TPPS monomer in the Q state, suggesting that the internal conversion from Q_y to Q_x states is much faster than that from B to Q_y states due to the small energy separation between two states.

3.3. Mesoscopic structure and spectral properties of TPPS J-aggregate by scanning probe microscopy

It has been widely proposed that TPPS forms one-dimensional (1D) linear aggregate in solution from the results of linear dichroism as depicted in Fig. 1 [4]. However, the direct observation of mesoscopic structure of TPPS J-aggregate is quite limited [32]. The spectral properties of aggregates should have strong correlation with their mesoscopic structures, and thus direct observation of spatially resolved spectroscopic property of mesoscopic structures is indispensable. We have conducted additional measurements to characterize the nanoscopic structures of TPPS aggregate as transferred on the substrate by means of atomic force microscopy and scanning near-field optical microscopy. Assemblies of TPPS were prepared on the surface of glass substrate by drop casting and spin coating. As for the reference, TPPS monomer transferred on the substrate with same procedure has also been examined.

A typically observed non-contact AFM image of TPPS J-aggregate is shown in Fig. 6a. The existence of J-aggregate is confirmed by the absorption spectrum of sample thin film. When the J-aggregate solution was spin coated on the substrate, very remarkable morphologies of aggregates were observed in its AFM image. The J-aggregate in thin film forms long and narrow rod-like structure. This corresponds well to the mesoscopic structure of the TPPS J-aggregate observed by Nagahara et al. in SNOM topographic image [32]. In some parts of the image, nano-rods agglutinate and form the cingulum of nano-rods. Although the length of the nano-rods extends in wide range from a few tens of nanometers to a micrometer, the dimension of the single nano-rod is rather uniform; the height and width of single nano-rod is ∼4 nm in height and ∼30 nm in width, respectively (Fig. 6c). The height of the crossing point of the nano-rods (8 nm), which is indicated by the white arrow in Fig. 6a, is twice as high as single nano-rod. Thus, 4 nm is considered to be the thickness of single nano-rod. However the width of the single nano-rod, ∼30 nm, is too larger for the lateral size of single TPPS molecule which is estimated to be ∼1.9 nm from the molecular modeling (see Fig. 1). Even if we take into account the convolution of the apex size of the AFM tip, the lateral size of single TPPS in AFM image could not reach to 30 nm. Structural dimension of nano-rod in AFM image implies that 1D aggregate of TPPS may be gathered to form nano-rod of TPPS J-aggregate. In fact, the nano-rods tend to agglutinate and form the cingulum of nano-rods. It should be noted that the J-aggregate components in aqueous solution can be filtrated with the membrane filter which has very small pore size such as 0.5 μm. The filtration induced the drastic diminution of the absorption peak of J-aggregate (not shown). This suggests that the agglutinated thick nano-rod is formed in solution phase. Nano-rod of J-aggregate can be assigned to the quasi two-dimensional aggregate structure. On the other hand, such kinds of rod-like structures cannot be

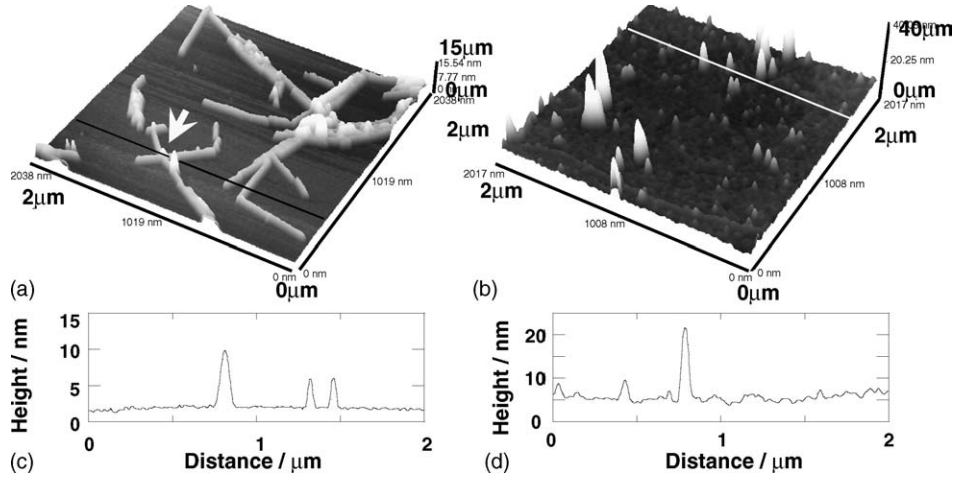

Fig. 6. AFM images for spin coated films of (a) J-aggregate and (b) monomer solution. (c and d) The topographic cross-section of J-aggregate and monomer thin film, respectively. Scan size of the AFM image is 2.0 μm × 2.0 μm.

observed in the thin film of TPPS monomer as illustrated in Fig. 6b. Instead, small microcrystalline protrusions with a few to a few tens of nanometer height and several tens of nanometers in lateral size are observed as in the cross-section shown in Fig. 6d.

In addition to the rod-like J-aggregate structure, we found different types of mesoscopic structures of J-aggregate by changing the film preparation method. The thin film prepared by drop casting of the sample solution shows microcrystal-like structures. The topographic image of microcrystalline structure of TPPS J-aggregate obtained by SNOM is depicted in Fig. 7a. The microcrystalline structures of J-aggregate have a few micrometers lateral dimension and the height reaches to 200 nm in some structure. In contrast to the nano-rod observed in spin coated film, microcrystalline structure is much larger than nano-rod structure. This structural difference probably depends on the drying process of the sample solution. In contrast to the deposition by spin coating, applied solution was left until drying up all the solvent in drop casting method. It takes more than half an hour to prepare the film because the films are prepared under ambient condition at room temperature. It is enough long for crystal growth at the solution/substrate interface. In addition to the agglutinative characteristics of TPPS J-aggregate observed in the AFM image in Fig. 6a, mean concentration increases during the evaporation of the solvent, which enhances the aggregation formation [8]. Thus, the large microcrystalline structure in the aggregate can be prepared by drop casting. A cross-section performed along the line is depicted in the topography in Fig. 7b. The height of the structures changes almost ∼50 nm unit, suggesting that the crystalline structures are formed by piling up the brick of TPPS J-aggregate.

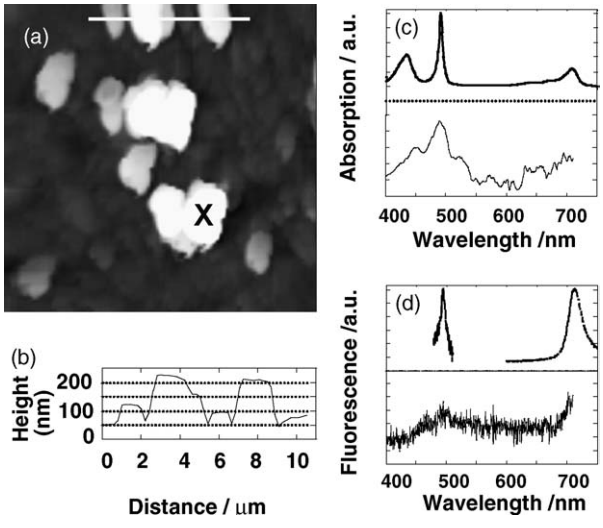

Fig. 7. (a) Topography of microcrystalline J-aggregate in thin film observed by SNOM. (b) The cross-sectional analysis of topography of microcrystalline structures measured along the white line in the image. The near-field (c) absorption and (d) fluorescence spectra of microcrystalline structure (lower panel with solid line) in position X are shown together with the corresponding spectrum in aqueous solution (upper panel with dotted line). The fluorescence spectrum was excited at 410 nm. Scan size of the topographic image is 20 μm × 20 μm.

A near-field absorption and fluorescence spectra of a microcrystal of TPPS J-aggregate have been demonstrated. We should note that both absorption and fluorescence spectra longer than 715 nm were cut by IR cut filter to avoid the interference of the shear-force diode laser that is utilized to control the tip–sample distance. In addition, the *B*-state fluorescence signal from the nano-rod of J-aggregate was too weak to get the signal under SNOM apparatus. It is due to the extremely low fluorescence quantum yield and the lack of physical amount of compound in thin film. The spectra were measured on top of the microcrystalline structure observed in drop-casted film of Fig. 7a, as indicated with "X" in the image. Lower panels in Fig. 7c and d depict the near-field absorption and fluorescence spectrum, respectively. The near-field spectra can be identified to J-aggregate because of the characteristic peaks of *B* and *Q* bands. The near-field absorption spectrum shows the main absorption peak at 490 nm as well as the spectrum obtained in the solution (Fig. 7c), although the peak width is very broad as compared with that observed in aqueous solution. This peak should correspond to the *B*-state absorption. The absorption spectrum shows the several peaks and valleys in addition to the absorption peak

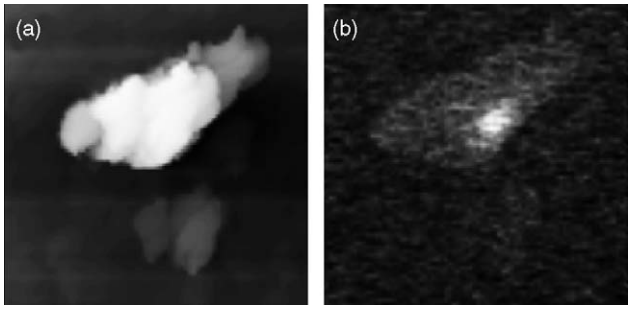

Fig. 8. (a) Topographic and (b) corresponding fluorescence images of TPPS cast-film observed at 510 nm. The sample was excited at 410 nm. Image was taken with 15 μm × 15 μm scan size.

of J-aggregate, which may be due to the interference of weak white-light continuum used as probe light. The near-field fluorescence spectrum shows weak but obvious fluorescence signal that has a peak at 500 nm and the increment of the intensity above 675 nm. From the comparison with the spectrum observed in aqueous solution (Fig. 7d, dashed line), the fluorescence peak at 500 nm and the increment above 675 nm can be assigned to the *B*-state fluorescence and high energy band edge of *Q*-state fluorescence of J-aggregate. Though the peaks are originated from the J-aggregate, the spectrum observed in near-field fluorescence spectrum is very broad as compared with that in aqueous solution. For both absorption and fluorescence, spectrum broadening of the peak is obviously observed. This can be explained by the structural inhomogeneity of inner structure of J-aggregate microcrystal. Microcrystals of J-aggregate are most probably constructed by the agglutination of the nano-rod of J-aggregates. From the comparison of the size, the microcrystalline structure is composed with large numbers of J-aggregate nano-rod. This will cause the structural inhomogeneity of microcrystal structures and results in the spectral broadening.

Finally we have examined the *B*-state fluorescence imaging of J-aggregate by SNOM. Fig. 8 shows the topographic picture of microcrystalline structure of TPPS J-aggregate and corresponding fluorescence image observed at 510 nm. A bright fluorescence spot was observed inside the slightly weak fluorescence image, which is not corresponding well to the shear-force topography of microcrystalline structure. This is probably due to the inhomogeneity inside the microcrystal. We also see very weak emission all over the observed area. This is probably the emission from the smaller microcrystalline structures around the large microcrystal observed in topographic image or very thin sediments of J-aggregate.

4. Conclusions

We have studied the fluorescence dynamics of TPPS in various forms by utilizing the femtosecond fluorescence upconversion spectroscopy as well as mesoscopic structures and spatially resolved spectroscopic properties of TPPS J-aggregate by means of SNOM. Femtosecond fluorescence lifetime measurements of *B* state revealed the very short fluorescence lifetime of all species of TPPS, and especially J-aggregate has very short lifetime of 140 ± 10 fs. In addition to the short *B*-state fluorescence lifetime, we have found very weak and fast decay component in TPPS monomer at shorter wavelength edge of the *Q*-band fluorescence. This very weak fluorescence can be assigned to the fluorescence originated from $Q_y(0, 0)$ state. The internal conversion from Q_y to Q_x states is estimated to be much faster than that from *B* to Q_y states from the analysis of this very fast component.

The analysis of the structures of J-aggregate by AFM and SNOM shows the different types of mesoscopic structures of TPPS J-aggregate, which are depending on the thin film preparation method. Under quick drying process, TPPS forms the nano-rod of the J-aggregate by interaction between 1D aggregate and form rather homogeneous quasi-2D rod-like structure. On the other hand, large microcrystalline structure is formed during the evaporation process in drop cast film. The broadening of the peaks in the near-field absorption and fluorescence spectra of microcrystalline structure indicate that the microcrystals are rather structurally inhomogeneous. *B*-state fluorescence imaging of J-aggregate was also demonstrated with SNOM.

Acknowledgement

This work was partially supported by Grant-in-Aid for Scientific Research on Priority Areas of Molecular Nano Dynamics, from MEXT, Japan.

References

[1] G. Schibe, Angew. Chem. 49 (1936) 563.
[2] E.E. Jelly, Nature 138 (1936) 1009.
[3] E.B. Fleisher, J.M. Palmer, T.S. Srivastava, A. Chatterjee, J. Am. Chem. Soc. 93 (1971) 3162.
[4] O. Ohno, Y. Kaizu, H. Kobayashi, J. Chem. Phys. 99 (1993) 4128.
[5] J.M. Ribó, J. Crusats, J.-A. Farrera, M.L. Valero, J. Chem. Soc. Chem. Commun. (1994) 681.
[6] D.L. Akins, S. Özçelik, H.-R. Zhu, C. Guo, J. Phys. Chem. 100 (1996) 14390.
[7] N.C. Maiti, M. Ravikanth, S. Mazumdar, N. Periasamy, J. Phys. Chem. B 99 (1995) 17192.
[8] A. Miura, K. Matsumura, X. Su, N. Tamai, Acta Phys. Pol. A. 94 (1998) 835–846.
[9] J. Deisenhofer, O. Epp, K. Miki, R. Huber, H. Michel, Nature 318 (1985) 618.
[10] G. McDermott, S.M. Prince, A.A. Freer, A.M. Hawthornthwaite-Lawless, M.Z. Papiz, R.J. Cogdell, N.W. Isaacs, Nature 374 (1995) 517.
[11] S. Okada, H. Segawa, J. Am. Chem. Soc. 125 (2003) 2792.
[12] E. Betzig, J.K. Trautman, T.D. Harris, J.S. Weiner, R.L. Kostelak, Science 251 (1991) 1468.
[13] A. Miura, Y. Yanagawa, N. Tamai, J. Microsc. 402 (2001) 401.
[14] A. Miura, Y. Yanagawa, N. Tamai, J. Microsc. 402 (2001) 425.
[15] D.A. Higgins, P.F. Barbara, J. Phys. Chem. 99 (1995) 3.
[16] D.A. Higgins, J. Kerimo, D.A.V. Bout, P.F. Barbara, J. Am. Chem. Soc. 118 (1996) 4049.
[17] M. Gouterman, in: D. Dolphin (Ed.), The Porphyrins, vol. III, Academic Press, New York, 1978 (Chapter 1).
[18] H. Chosrowjan, S. Taniguchi, T. Okada, S. Takagi, T. Arai, K. Tokumaru, Chem. Phys. Lett. 242 (1995) 644.
[19] G.G. Gurzadyan, T.-H. Tran-Thi, T. Gustavsson, J. Chem. Phys. 108 (1998) 385.
[20] S. Akimoto, T. Yamazaki, I. Yamazaki, A. Osuka, Chem. Phys. Lett. 309 (1999) 177.

[21] H. Kano, T. Kobayashi, J. Chem. Phys. 116 (2002) 184.
[22] I.L. Arbeloa, K.K. Rohatgi-Mukherjee, Chem. Phys. Lett. 128 (1986) 474.
[23] P.R. Bevington, Data Reduction and Error Analysis for the Physical Sciences, McGraw-Hill, NY, 1969.
[24] K. Kalyanasundaram, M. Neumann-Spallart, J. Phys. Chem. 86 (1982) 5163.
[25] H. Khun, J. Chem. Phys. 53 (1969) 101.
[26] T. Kobayashi, J-Aggregates, World Scientific, Singapore, 1996.
[27] S.D. Bore, D.A. Wiersma, Chem. Phys. Lett. 165 (1990) 45.
[28] F.C. Spano, J.R. Kuklinski, S. Mukamel, J. Chem. Phys. 94 (1991) 7534.
[29] E.O. Potma, D.A. Wiersma, J. Chem. Phys. 108 (1998) 4894.
[30] H. Fidder, J. Knoestar, D.A. Wiersma, Chem. Phys. Lett. 171 (1990) 529.
[31] H. Fidder, D.A. Wiersma, Phys. Status Solidi B 188 (1995) 285.
[32] T. Nagahara, K. Imura, H. Okamoto, Scanning 26 (2004) I-10.